THERMALLY INDUCED GRABEN IN PEAK-RING BASINS AND GHOST CRATERS ON MERCURY. David M. Blair[1], Andrew M. Freed[1], Paul K. Byrne[2], Christian Klimczak[2], Sean C. Solomon[2], Thomas R. Watters[3], Louise M. Prockter[4], H. Jay Melosh[1], and Maria T. Zuber[5]. [1]Department of Earth and Atmospheric Sciences, Purdue University, West Lafayette, IN 47907, USA, dblair@purdue.edu; [2]Department of Terrestrial Magnetism, Carnegie Institution of Washington, Washington, DC 20015, USA; [3]Center for Earth and Planetary Studies, National Air and Space Museum, Smithsonian Institution, Washington, DC 20560, USA; [4]The Johns Hopkins University Applied Physics Laboratory, 11100 Johns Hopkins Road, Laurel, MD 20723, USA; [5]Department of Earth, Atmospheric, and Planetary Sciences, Massachusetts Institute of Technology, Cambridge, MA 02139, USA.

Introduction: MESSENGER has documented large graben inside several impact basins on Mercury, including the peak-ring basins Rachmaninoff, Raditladi, and Mozart [1], the buried ("ghost") impact basins and craters of Mercury's northern plains [2], and the larger Caloris and Rembrandt basins [3, 4]. Here, we focus on the first two environments, where graben are located within smooth volcanic plains and often display concentric patterns. What caused these graben to form, and why do these interior patterns of graben occur only on Mercury? Here we attempt to answer these questions through numerical modeling of several candidate scenarios.

Observational Constraints: The peak-ring basins Rachmaninoff, Raditladi, and Mozart (diameters $D \sim 290$, 250, and 225 km, respectively) all contain the same basic graben distribution: a central region devoid of graben (but containing wrinkle ridges in Rachmaninoff and Mozart), followed outward by a broad band dominated by concentric graben, and then a zone of graben in more polygonal patterns toward the inner edge of the peak ring (Fig. 1a). In the northern plains, the most prominent graben occur in ghost craters ($D < 150$ km) nested within larger ghost basins ($D > 150$ km) such as Goethe basin (Fig. 1b). Graben in these nested ghost craters typically form large polygonal patterns at their centers and display more radial orientations farther out and circumferential orientations near the buried rim. Some ghost craters also contain small circular graben (10–15 km across), which may have radial graben extending outward from the circle in ray-like patterns (Fig. 1c).

The orientation of a graben depends on the stress state at the time of formation. If basin-circumferential stresses are more extensional than basin-radial stresses, radial graben will form. If instead radial stresses are more extensional, circumferential graben will form. When radial and circumferential stresses are approximately equal, the orientation of a given fault will depend on local structure, and polygonal patterns can emerge.

Testing of Candidate Scenarios: We used thermomechanical, viscoelastic finite element models to test three types of processes (uplift, subsidence, and thermal contraction) under a variety of conditions and subsurface geometries. For each model we calculated the resulting steady-state stresses and compared them with the stresses inferred from the observed style of faulting.

Uplift of the crater floor. Uplift can be caused by several different processes, all of which lead to extensional stresses throughout much of the basin. Graben observed within the Caloris basin have been attributed to uplift associated with isostatic re-adjustment [5],

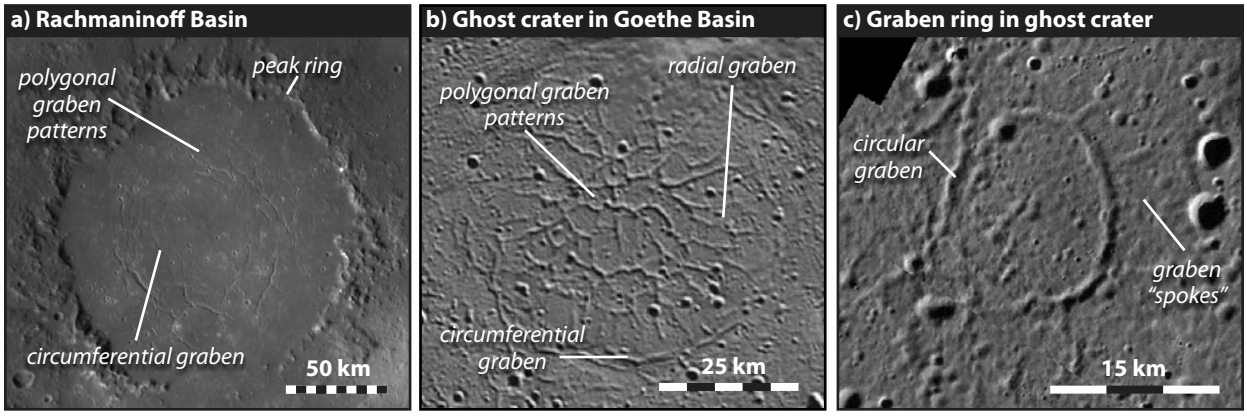

Figure 1. (a) The area within the peak ring of Rachmaninoff basin, showing the central region without graben, the zone of circumferential graben, and the transition to graben in polygonal patterns. (b) A ghost crater within Goethe basin in Mercury's northern plains, with polygonal patterns at its center, radial graben farther out, and crater-rim circumferential graben. (c) A graben ring within a different ghost crater, showing a pattern of a single circular graben with radial graben extending outwards.

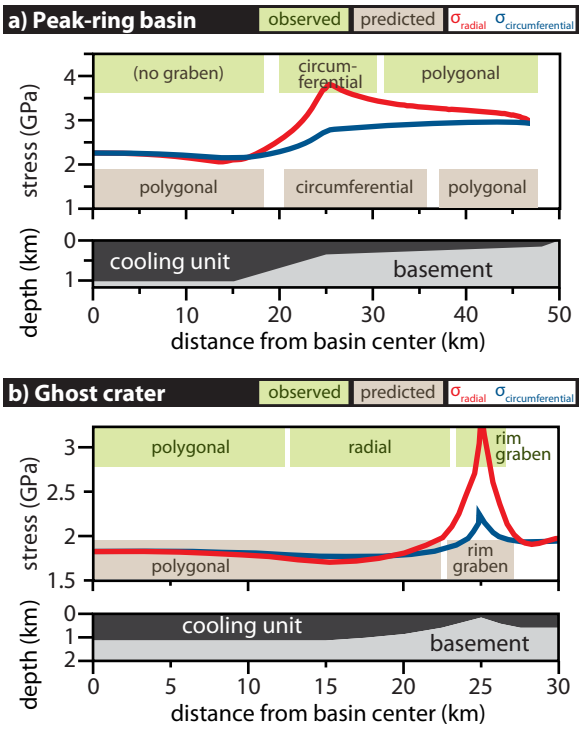

Figure 2. Stresses from thermal contraction, shown above the fill geometry used to generate that stress field. Note that stresses are in the > 1 GPa range because we do not model rock failure; the magnitude of these stresses only indicates a substantial potential for faulting. (a) Best-fit model for peak-ring basins (note that the peak ring is at a radius of ~50 km and is not shown). (b) Best-fit model for a ghost crater.

lower crustal flow [6], and exterior loading [7]. Our models show that basin floor uplift is incapable of producing the required stress state, as this mechanism does not lead to the formation of circumferentially oriented graben.

Subsidence due to volcanic loading. When the center of a basin is loaded by volcanic material, the additional overburden causes subsidence and compression at the basin center and uplift and extension in the forebulge. This mechanism has been invoked to explain graben near the outer edges of lunar mare basins [e.g. 8, 9]. Our models indicate that subsidence can lead to graben within a basin only if we assume an implausibly thin lithosphere (< 5 km) and a center-heavy load distribution. Such graben would still be radially oriented.

Thermal contraction of volcanic fill. The volcanic materials filling the peak-ring basins and burying the ghost basins and craters contract as they cool, generating extensional stresses. The resulting stress state is highly dependent on the geometry of the fill, as an uneven basement floor can induce bending stresses that cause the two lateral stress components to differ in magnitude (Fig. 2). This effect can account for circumferential graben within the peak-ring basins and over the buried rims of ghost craters, and cooling can also account for the polygonal patterns of graben observed in both environments. The inferred 'stair-step' basement floor geometry for the peak-ring basins is similar to structures observed in seismic imaging of Chicxulub crater [10]. In areas where circumferential graben have accommodated extensional radial stresses, the remaining stress state will be dominated by circumferential extensional stress, which could account for the pattern shown in Fig. 1c.

Conclusions: We find that thermal contraction of the smooth plains unit is the most likely cause of the observed graben patterns. By considering variations in the basement floor geometry below the cooling volcanic unit, we can fully match the patterns observed within ghost craters of the northern plains, and match most of the pattern in the peak-ring basins. However, all geometries predict that polygonal patterns of graben will form in the centers of the peak-ring basins, and such features are not observed. One possibility is that a thin late-stage flow covered the central area of the peak-ring basins after the smooth plains were mostly cool. An observation of partially filled graben would support this hypothesis, but higher-resolution images than are currently available will be needed to test this idea fully. Another implication of this scenario is that at least a portion of the smooth plains in all of the peak-ring basins must be volcanic in origin, as impact melt cannot account for a late-stage covering flow.

Cooling stresses should be ubiquitous in any crater that is filled with volcanic materials, or those with substantial amounts of impact melt. Why, then, are these interior graben patterns seen only on Mercury? The answer may lie in the unusual properties of lava flows on Mercury (including high effusion rates and low viscosities [4, 11]), which favor pooling within basins and enable the development of wide graben during cooling. In contrast, lunar mare basins generally contain a series of relatively thin asymmetric flows that likely lead to pervasive cracking during cooling rather than large interior graben.

References: [1] Prockter, L. M. et al. (2011) *GSA Abstracts with Programs 43,* 359. [2] Head, J. W. et al. (2011) *Science 333*, 1853. [3] Watters, T. R. et al. (2009) *EPSL 285,* 309. [4] Watters, T. R. et al. (2009) *Science 324*, 618. [5] Dzurisin, D. (1978) *JGR 83,* 4883. [6] Watters, T. R. et al. (2005) *Geology 33*, 669. [7] Kennedy, P. J. et al. (2008) *JGR 113*, E08004. [8] Melosh, H. J. (1978) *Proc. Lunar Planet. Sci. Conf. 9th*, 3513. [9] Freed, A. M. et al. (2001) *JGR 106,* 20603. [10] Morgan, J. V. et al. (2000) *EPSL 5660,* 1. [11] Nittler, L. R. et al. (2011) *Science 333*, 1847.